ChemComm

COMMUNICATION

View Article Online
View Journal | View Issue

Cite this: *Chem. Commun.*, 2015, **51**, 15386

Received 22nd July 2015,
Accepted 25th August 2015

DOI: 10.1039/c5cc06128h

www.rsc.org/chemcomm

A π-electron deficient diaminotriazine functionalized MOF for selective sorption of benzene over cyclohexane†

Biplab Manna,‡[a] Soumya Mukherjee,‡[a] Aamod V. Desai,[a] Shivani Sharma,[a] Rajamani Krishna[b] and Sujit K. Ghosh*[a]

A diaminotriazine functionalized novel MOF (DAT-MOF-1) has been synthesized stemming out of a π-electron-deficient pore-surface functionalization based linker-design principle, which results in efficient selectivity of benzene sorption over its aliphatic analogue cyclohexane, crucial from the industrial standpoint.

Metal–organic frameworks (MOFs), formed by the coordination chemistry-assisted self-assembly process of organic linkers and metal ions, have evolved as one of the most preferred new-generation materials, owing to their superlative potential in multifarious fields, such as gas storage, chemical separation, sensing, drug delivery, and catalysis.[1] These crystalline materials score over the other classes of functional materials because of a few unique advantages, such as their unique periodical structures with long-range order, excellent porosity, framework flexibility, and tunable pore surface functionalization, which endow them with promising storage and separation applications.[2] Among the diverse porous adsorbent materials utilized for serving efficient separation of flue gas and hydrocarbons, MOFs have established themselves as a uniquely promising class of functional adsorbents owing to the unmatched unison of their aforementioned characteristics.[3]

From the application perspective, the separation of liquid phase hydrocarbons, especially those having similar physical properties and comparable molecular sizes, is highly challenging for industrial applications. In this context, the industrially crucial separation of benzene (Bz) and cyclohexane (Cy) poses a challenge. The recognized difficulty behind this C_6 hydrocarbon stream separation originates as a consequence of the unavoidable production of cyclohexane during the catalytic hydrogenation of benzene in the benzene/cyclohexane miscible system and also due to their considerably close boiling points (benzene, 353.25 K; cyclohexane, 353.85 K: Table S1, ESI†), similar molecular volumes, comparable Lennard-Jones collision diameters along with low relative volatilities.[4] While close proximity in their boiling points (difference: 0.6 K) rules out conventional fractional distillation methods, specialized distillation protocols such as azeotropic and extractive distillation methods employed with entrainer species such as sulpholane, dimethylsulfoxide, *N*-methylpyrrolidone, and *N*-formylmorpholine involve high energy-intensive requirements. On the contrary, adsorptive separation offers an energy-efficient alternative to extractive distillation, especially for Bz/Cy mixtures containing small percentages of benzene, as is commonly encountered.

Interesting enough, these two analogue species have distinct spatial configurational orientations; benzene is a planar π-cloud entity, while aliphatic cyclohexane exists in either chair or boat configuration (Fig. S1, ESI†). This inherent dissimilarity might seem to be the imperative key factor behind efficiently separating the duo (Scheme 1). The favourable role of π-complexation with benzene behind the selective sorption-mediated Bz/Cy separation was explored in cation-exchange Faujasite-type zeolites Na-Y, Pd-Y, Ag-Y, and FAU-type zeolite membranes;[5] while

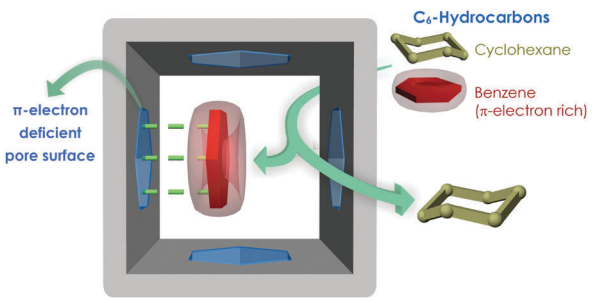

Scheme 1 Schematic representation of the strategic employment of π-electron deficient diaminotriazine (DAT)-functionalized pore surface for exhibiting a selective interplay with benzene over cyclohexane.

[a] *Indian Institute of Science Education and Research (IISER), Dr. Homi Bhabha Road, Pashan, Pune, 411008, India. E-mail: sghosh@iiserpune.ac.in; Fax: +91 20 2589 8022; Tel: +91 20 2590 8076*

[b] *Van't Hoff Institute for Molecular Sciences, University of Amsterdam, Science Park 904, 1098 XH Amsterdam, The Netherlands*

† Electronic supplementary information (ESI) available. CCDC 1414256. For ESI and crystallographic data in CIF or other electronic format see DOI: 10.1039/c5cc06128h

‡ B.M. and S.M. have contributed equally.

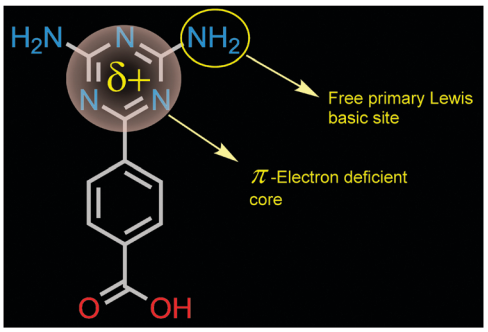

Fig. 1 Structure of the π–e⁻ deficient triazine (DAT) core based linker (LH), with Lewis basic primary amino groups, imparting framework functionalization.

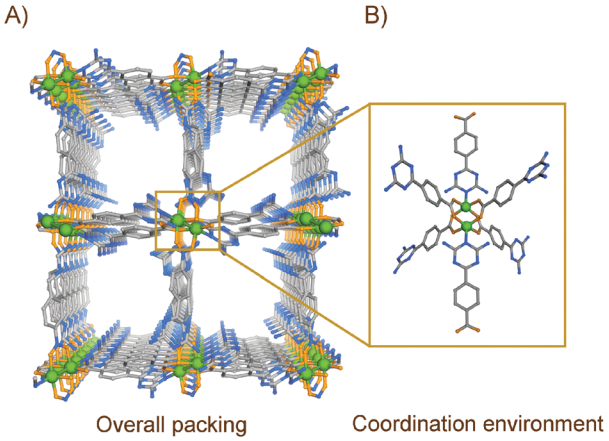

Fig. 2 (a) Perspective view of the overall packing of DAT-MOF-1a (guest molecules and H atoms are omitted for clarity); (b) Lewis basic N-rich π-electron deficient coordination environment constructing DAT-MOF-1a, rendering channel functionalization.

recent years have witnessed some porous MOF materials being used for the targeted selective sorption based separation of Bz/Cy.[4b,c,6] However, the ligand design-strategy derived achievement of such separation performance is indeed scarce.[4b,6g]

Ligand functionalization based attainment of excellent separation performance by MOFs has witnessed remarkable upsurge in recent times, markedly motivated by the pioneering work of Chen *et al.*[7] Over the years, the triazine core has been quite well-harnessed chiefly by Zhou *et al.*, as constituent linkers in the MOF domain for presenting excellent adsorption features with concomitant thermal robustness of the materials.[8] Under this backdrop, we intended to achieve Bz/Cy separation by the favourable π–π stacking driven interplay of the π-electron deficient triazine core of the employed rigid carboxylate linker (Fig. 1) functionalized MOF pore surface and π-rich guest species benzene.[9] Herein, for the first time, the electron deficient diaminotriazine (DAT) core of a new-fangled rigid monocarboxylic acid linker has been proficiently exploited for imparting essential π-electron deficiency to the ensuing new MOF (DAT-MOF-1) for achieving the targeted selective sorption-based separation of benzene over cyclohexane at ambient temperature (298 K) and pressure (1 atm). The electrostatic surface potential (ESP) plot (Fig. S2, ESI†) for the conceived linker was verified to have significant π-electron deficiency, which makes its choice strategically triggered. Upon reaction of ligand (LH) (Fig. S3, ESI†) and $Cu(NO_3)_2{\cdot}3H_2O$ under solvothermal conditions in the binary solvent system DMF/MeOH (1 : 1), block shaped green shiny single crystals of compound DAT-MOF-1a $[\{Cu(L)_2\}{\cdot}xG]_n$ (G refers to disordered guest molecules) are obtained (Fig. S7, ESI†). A single-crystal X-ray diffraction (SC-XRD) study of the compound showed the formation of a two-dimensional (2D) network, which upon further hydrogen bond formation with similar 2D networks in proximity gave rise to intermolecular hydrogen bonded three-dimensional (3D) supramolecular networks (DAT-MOF-1a) (Fig. 2), crystallized in the orthorhombic space group *Pbnb*. The *Adsym* subroutine of PLATON was applied to confirm that no additional symmetry could be applied to the model. The asymmetric unit contains one Cu(II) center and two monocarboxylate DAT (deprotonated form of LH) linkers. Nearly five guest DMF molecules detected by the combined inputs of elemental analysis (ESI†), IR spectral investigation and thermogravimetric analysis (Fig. S8 and S17, ESI†) could not be located in the asymmetric unit from Fourier maps in the refinement cycles, because of a high extent of disorder for these moieties in the crystal. The phase purity for the as-synthesized phase was confirmed by the PXRD analyses (Fig. S18, ESI†) coupled with the SC-XRD-based unit cell analysis of arbitrarily chosen crystals from the bulk phase.

As observed from the perspective view of the supramolecular H-bonded 3D-framework, the pores along the *a*-axis (Fig. S11–S14, ESI†) of dimensions $\sim 6.71 \times 7.08$ Å^2 are well-decorated with Lewis basic pyridyl and primary amine functionalities, which should ideally facilitate strong interactions with polar guest species CO_2 owing to the latter's high quadruple moment (-13.4×10^{-40} C m^2)[10] over its congener flue gases.[1a,11] The anticipated CO_2-selective adsorption feature was indeed verified for the activated form of DAT-MOF-1a, namely DAT-MOF-1, as evident from the single component gas adsorption isotherms recorded at low temperatures (77 K and 195 K). Exclusively for CO_2, there was a distinct two step-mediated adsorption uptake observed with noteworthy hysteresis (typical signature of dynamic frameworks) (Fig. S20, ESI†), owing to the concomitant host–guest interaction-driven dynamic structural transformations or breathing phenomena, accompanying the CO_2 vapour sorption process.[12] A prominent two-step sorption profile and the observed hysteretic desorption can be attributed to structural transitions between relatively open and closed framework structures as CO_2 adsorptive gets adsorbed with substantial hysteresis consequential from the metastability of the more open structure, similar to the previous reports on breathing phenomena exhibited by soft porous crystalline frameworks.[12a,13] On the flipside, no such steps were observed for the CO_2 sorption isotherm at 298 K over a similar pressure range (Fig. S21, ESI†), validating the dependency factor of the structural transitions accompanying the sorption process on the low temperature-mediated specific interactions of the host framework with guest CO_2 molecules. The guest-free nature and excellent crystalline features of the activated phase DAT-MOF-1 were once confirmed from the thermogravimetric analyses (TGA) and Powder X-ray Diffraction (PXRD) profiles respectively

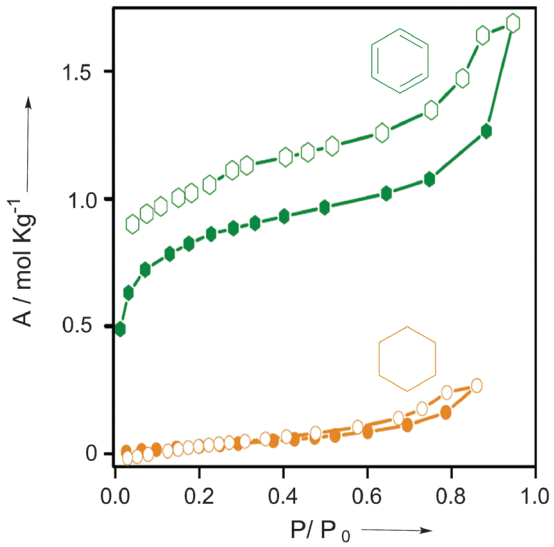

Fig. 3 Solvent sorption isotherms of compound DAT-MOF-1 recorded at 298 K for Bz and Cy. Closed and open symbols denote adsorption and desorption, respectively.

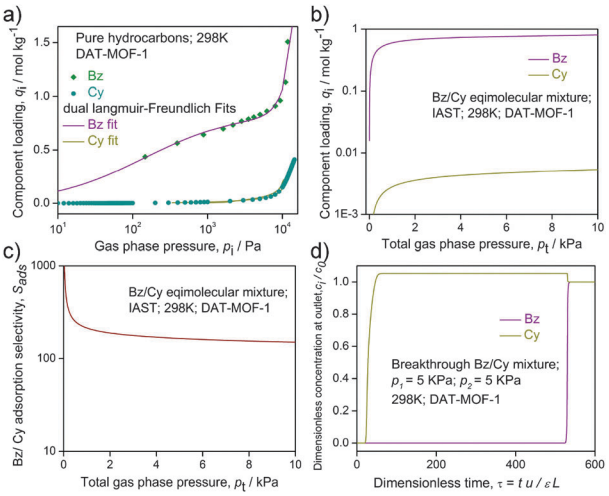

Fig. 4 (a) Comparison of experimental data for pure component isotherms for Bz and Cy in DAT-MOF-1 with dual-Langmuir–Freundlich fits that are shown by the continuous solid lines; (b) IAST calculations for Bz uptake capacity for equimolar Bz/Cy mixtures in DAT-MOF-1; (c) IAST calculations of adsorption selectivity for equimolar mixtures of Bz/Cy in DAT-MOF-1; (d) breakthrough simulations for Bz/Cy in a fixed bed of DAT-MOF-1 at 298 K.

(Fig. S17 and S18, ESI†), and the same was harnessed for the targeted selective vapor sorption based separation studies of benzene/cyclohexane.

Substantiating the anticipated selective interplay of Bz with DAT-MOF-1, the single component vapor sorption experiments for both the solvents Bz and Cy when measured at 298 K, the striking difference between their respective uptake amounts (1.5 mol kg^{-1} for Bz, while only $\sim$0.2 mol kg^{-1} for CY) was revealed (Fig. 3 and Fig. S22, ESI†). ^{13}C NMR studies performed using the DCl/DMSO-d_6 digested samples after vapor exposure to the Bz and Cy solvent vapors and their 1 : 1 equimolar mixtures indubitably revealed exclusive Bz-selectivity (Fig. S23, ESI†).

We evaluate Bz/Cy separation by utilizing the Ideal Adsorbed Solution Theory (IAST) calculations. Fig. 4a shows the experimental data for pure component isotherms of Bz and Cy in DAT-MOF-1; the continuous solid lines are Langmuir–Freundlich fits (the fit parameters being specified in Table S2, ESI†). For fitting purposes, the sorption branches of the isotherms were solely considered. Fig. 4b shows IAST calculations of Bz uptake capacity for equimolar Bz/Cy mixtures in DAT-MOF-1. Notably, for pressures exceeding about 1 kPa, the adsorbed phase contains predominantly Bz. Fig. 4c presents IAST calculations for adsorption selectivity, S_{ads}, for equimolar Bz/Cy mixtures with values in excess of about 200, suggesting the viability of the present MOF material for vapor phase selective sorption based Bz/Cy separation at 298 K. Transient breakthrough simulations, using the established methodology described in earlier work,[14] confirm that sharp separations are obtained in a fixed bed adsorber; see Fig. 4d. The video animation-illustration (accompanied as ESI†) evidently demonstrates that DAT-MOF-1 has both significantly higher selectivity and uptake for Bz over Cy.

In a nutshell, as a first-of-its kind convergent approach, the triazine core's π-electron-deficiency coupled with the mutual attendance of amino moieties for the reported DAT-MOF-1 has been strategically exploited for the achievement of selective benzene sorption over its aliphatic analogue cyclohexane. Further investigations to consolidate its practical applications in terms of realistic industrial separation scenario are currently underway. This might indeed help to develop functional porous materials by virtue of their tunable functionalities; immensely important for exhibiting industrially crucial hydrocarbon separation features.

B.M. is thankful to CSIR for research fellowship, while IISER Pune is acknowledged for the same from S.M., A.V.D. and S.S.; DST (Project No. GAP/DST/CHE-12-0083) and DST-FIST (SR/FST/CSII-023/2012) are acknowledged for generous financial support.

Notes and references

1 (*a*) Z. Zhang, Y. Zhao, Q. Gong, Z. Li and J. Li, *Chem. Commun.*, 2013, **49**, 653; (*b*) Z. Zhang, Z.-Z. Yao, S. Xiang and B. Chen, *Energy Environ. Sci.*, 2014, **7**, 2868; (*c*) J.-R. Li, Y. Ma, M. C. McCarthy, J. Sculley, J. Yu, H.-K. Jeong, P. B. Balbuena and H.-C. Zhou, *Coord. Chem. Rev.*, 2011, **255**, 1791; (*d*) J.-R. Li, J. Sculley and H.-C. Zhou, *Chem. Rev.*, 2012, **112**, 869; (*e*) Z. Hu, B. J. Deibert and J. Li, *Chem. Soc. Rev.*, 2014, **43**, 5815; (*f*) S. S. Nagarkar, B. Joarder, A. K. Chaudhari, S. Mukherjee and S. K. Ghosh, *Angew. Chem., Int. Ed.*, 2013, **52**, 2881; (*g*) R. C. Huxford, J. Della Rocca and W. Lin, *Curr. Opin. Chem. Biol.*, 2010, **14**, 262; (*h*) P. Horcajada, R. Gref, T. Baati, P. K. Allan, G. Maurin, P. Couvreur, G. Férey, R. E. Morris and C. Serre, *Chem. Rev.*, 2012, **112**, 1232; (*i*) J. Lee, O. K. Farha, J. Roberts, K. A. Scheidt, S. T. Nguyen and J. T. Hupp, *Chem. Soc. Rev.*, 2009, **38**, 1450; (*j*) J. Gascon, A. Corma, F. Kapteijn and F. X. Llabrés i Xamena, *ACS Catal.*, 2014, **4**, 361.

2 (*a*) M. P. Suh, H. J. Park, T. K. Prasad and D.-W. Lim, *Chem. Rev.*, 2012, **112**, 782; (*b*) J. L. C. Rowsell and O. M. Yaghi, *Microporous Mesoporous Mater.*, 2004, **73**, 3; (*c*) M. J. Rosseinsky, *Nat. Mater.*, 2010, **9**, 609; (*d*) S. Mukherjee, B. Joarder, A. V. Desai, B. Manna, R. Krishna and S. K. Ghosh, *Inorg. Chem.*, 2015, **54**, 4403; (*e*) S. Mukherjee, B. Joarder, B. Manna, A. V. Desai, A. K. Chaudhari and S. K. Ghosh, *Sci. Rep.*, 2014, **4**, 5761.

3 (*a*) Z. Kang, M. Xue, L. Fan, L. Huang, L. Guo, G. Wei, B. Chen and S. Qiu, *Energy Environ. Sci.*, 2014, **7**, 4053; (*b*) B. Li, H.-M. Wen,

H. Wang, H. Wu, M. Tyagi, T. Yildirim, W. Zhou and B. Chen, *J. Am. Chem. Soc.*, 2014, **136**, 6207; (*c*) B. Li, H.-M. Wen, W. Zhou and B. Chen, *J. Phys. Chem. Lett.*, 2014, **5**, 3468; (*d*) I. Senkovska and S. Kaskel, *Chem. Commun.*, 2014, **50**, 7089; (*e*) Z. R. Herm, E. D. Bloch and J. R. Long, *Chem. Mater.*, 2014, **26**, 323; (*f*) Z. R. Herm, B. M. Wiers, J. A. Mason, J. M. van Baten, M. R. Hudson, P. Zajdel, C. M. Brown, N. Masciocchi, R. Krishna and J. R. Long, *Science*, 2013, **340**, 960.

4 (*a*) Y. Bai, J. Qian, Q. Zhao, Y. Xu and S. Ye, *J. Appl. Polym. Sci.*, 2006, **102**, 2832; (*b*) S. Shimomura, S. Horike, R. Matsuda and S. Kitagawa, *J. Am. Chem. Soc.*, 2007, **129**, 10990; (*c*) J.-P. Zhang and X.-M. Chen, *J. Am. Chem. Soc.*, 2008, **130**, 6010; (*d*) H. Dong, X. Yang, G. Yue, W. Cao and J. Zhang, *J. Chem. Eng. Data*, 2011, **56**, 2664.

5 (*a*) A. Takahashi and R. T. Yang, *AIChE J.*, 2002, **48**, 1457; (*b*) D. Barthomeuf and B.-H. Ha, *J. Chem. Soc., Faraday Trans. 1*, 1973, **69**, 2147; (*c*) B.-H. Jeong, Y. Hasegawa, K.-I. Sotowa, K. Kusakabe and S. Morooka, *J. Membr. Sci.*, 2003, **213**, 115.

6 (*a*) G. Li, C. Zhu, X. Xi and Y. Cui, *Chem. Commun.*, 2009, 2118; (*b*) J.-B. Lin, J.-P. Zhang, W.-X. Zhang, W. Xue, D.-X. Xue and X.-M. Chen, *Inorg. Chem.*, 2009, **48**, 6652; (*c*) R. Yang, L. Li, Y. Xiong, J.-R. Li, H.-C. Zhou and C.-Y. Su, *Chem. – Asian J.*, 2010, **5**, 2358; (*d*) S. Shimomura, R. Matsuda and S. Kitagawa, *Chem. Mater.*, 2010, **22**, 4129; (*e*) Y. Hijikata, S. Horike, M. Sugimoto, H. Sato, R. Matsuda and S. Kitagawa, *Chem. – Eur. J.*, 2011, **17**, 5138; (*f*) G. Ren, S. Liu, F. Ma, F. Wei, Q. Tang, Y. Yang, D. Liang, S. Li and Y. Chen, *J. Mater. Chem.*, 2011, **21**, 15909; (*g*) B. Joarder, S. Mukherjee, A. K. Chaudhari, A. V. Desai, B. Manna and S. K. Ghosh, *Chem. – Eur. J.*, 2014, **20**, 15303; (*h*) C.-X. Ren, L.-X. Cai, C. Chen, B. Tan, Y.-J. Zhang and J. Zhang, *J. Mater. Chem. A*, 2014, **2**, 9015; (*i*) A. Karmakar, A. V. Desai, B. Manna, B. Joarder and S. K. Ghosh, *Chem. – Eur. J.*, 2015, **21**, 7071; (*j*) J.-Y. Cheng, P. Wang, J.-P. Ma, Q.-K. Liu and Y.-B. Dong, *Chem. Commun.*, 2014, **50**, 13672.

7 (*a*) T.-L. Hu, H. Wang, B. Li, R. Krishna, H. Wu, W. Zhou, Y. Zhao, Y. Han, X. Wang, W. Zhu, Z. Yao, S. Xiang and B. Chen, *Nat. Commun.*, 2015, **6**, 7328; (*b*) Y. He, Z. Zhang, S. Xiang, F. R. Fronczek, R. Krishna and B. Chen, *Chem. Commun.*, 2012, **48**, 6493; (*c*) S.-C. Xiang, Z. Zhang, C.-G. Zhao, K. Hong, X. Zhao, D.-R. Ding, M.-H. Xie, C.-D. Wu, M. C. Das, R. Gill, K. M. Thomas and B. Chen, *Nat. Commun.*, 2011, **2**, 204.

8 (*a*) D. Sun, S. Ma, Y. Ke, T. M. Petersen and H.-C. Zhou, *Chem. Commun.*, 2005, 2663; (*b*) D. Sun, S. Ma, Y. Ke, D. J. Collins and H.-C. Zhou, *J. Am. Chem. Soc.*, 2006, **128**, 3896; (*c*) D. Sun, Y. Ke, D. J. Collins, G. A. Lorigan and H.-C. Zhou, *Inorg. Chem.*, 2007, **46**, 2725; (*d*) S. Ma, D. Sun, M. Ambrogio, J. A. Fillinger, S. Parkin and H.-C. Zhou, *J. Am. Chem. Soc.*, 2007, **129**, 1858; (*e*) W. Gao, F. Xing, D. Zhou, M. Shao and S. Zhu, *Inorg. Chem. Commun.*, 2011, **14**, 601.

9 H. Ren, T. Ben, E. Wang, X. Jing, M. Xue, B. Liu, Y. Cui, S. Qiu and G. Zhu, *Chem. Commun.*, 2010, **46**, 291.

10 (*a*) C. Graham, J. Pierrus and R. E. Raab, *Mol. Phys.*, 1989, **67**, 939; (*b*) A. D. Buckingham and R. L. Disch, *Proc. R. Soc. A*, 1963, **273**, 275.

11 (*a*) A. R. Millward and O. M. Yaghi, *J. Am. Chem. Soc.*, 2005, **127**, 17998; (*b*) S. Couck, J. F. M. Denayer, G. V. Baron, T. Rémy, J. Gascon and F. Kapteijn, *J. Am. Chem. Soc.*, 2009, **131**, 6326; (*c*) A. Demessence, D. M. D'Alessandro, M. L. Foo and J. R. Long, *J. Am. Chem. Soc.*, 2009, **131**, 8784; (*d*) T. M. McDonald, D. M. D'Alessandro, R. Krishna and J. R. Long, *Chem. Sci.*, 2011, **2**, 2022; (*e*) P. Pachfule, Y. Chen, J. Jiang and R. Banerjee, *J. Mater. Chem.*, 2011, **21**, 17737.

12 (*a*) S. Horike, S. Shimomura and S. Kitagawa, *Nat. Chem.*, 2009, **1**, 695; (*b*) C. Serre, F. Millange, C. Thouvenot, M. Noguès, G. Marsolier, D. Louër and G. Férey, *J. Am. Chem. Soc.*, 2002, **124**, 13519; (*c*) D. Dubbeldam, R. Krishna and R. Q. Snurr, *J. Phys. Chem. C*, 2009, **113**, 19317.

13 (*a*) C. Serre, F. Millange, C. Thouvenot, M. Noguès, G. Marsolier, D. Louër and G. Férey, *J. Am. Chem. Soc.*, 2002, **124**, 13519; (*b*) C. Serre, S. Bourrelly, A. Vimont, N. A. Ramsahye, G. Maurin, P. L. Llewellyn, M. Daturi, Y. Filinchuk, O. Leynaud, P. Barnes and G. Férey, *Adv. Mater.*, 2007, **19**, 2246; (*c*) Y. Yue, J. A. Rabone, H. Liu, S. M. Mahurin, M.-R. Li, H. Wang, Z. Lu, B. Chen, J. Wang, Y. Fang and S. Dai, *J. Phys. Chem. C*, 2015, **119**, 9442.

14 R. Krishna, *RSC Adv.*, 2015, **5**, 52269.

Supporting Information

A π-electron Deficient Diaminotriazine Functionalized MOF For Selective Sorption of Benzene Over Cyclohexane

Biplab Manna,[1,‡] Soumya Mukherjee, [1,‡] Aamod V.Desai,[1] Shivani Sharma,[1] Rajamani Krishna,[2] and Sujit K.Ghosh[1]*

[1]Indian Institute of Science Education and Research (IISER), Pashan, Pune, Maharashtra 411008, India

[2]Van 't Hoff Institute for Molecular Sciences, University of Amsterdam, Science Park 904, 1098 XH Amsterdam, The Netherlands

***E-mail:** sghosh@iiserpune.ac.in **Fax:** +91-20-25898022 **Tel:** +91-20- 25908076*

Table of Contents

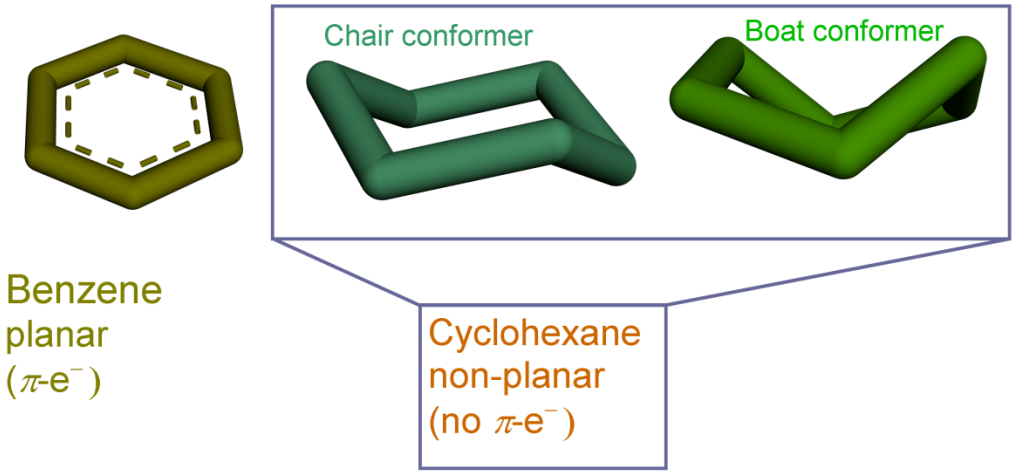

Figure S1: General conformations of planar aromatic Benzene (Bz) (left) and non-planar aliphatic Cyclohexane (Cy) (right).

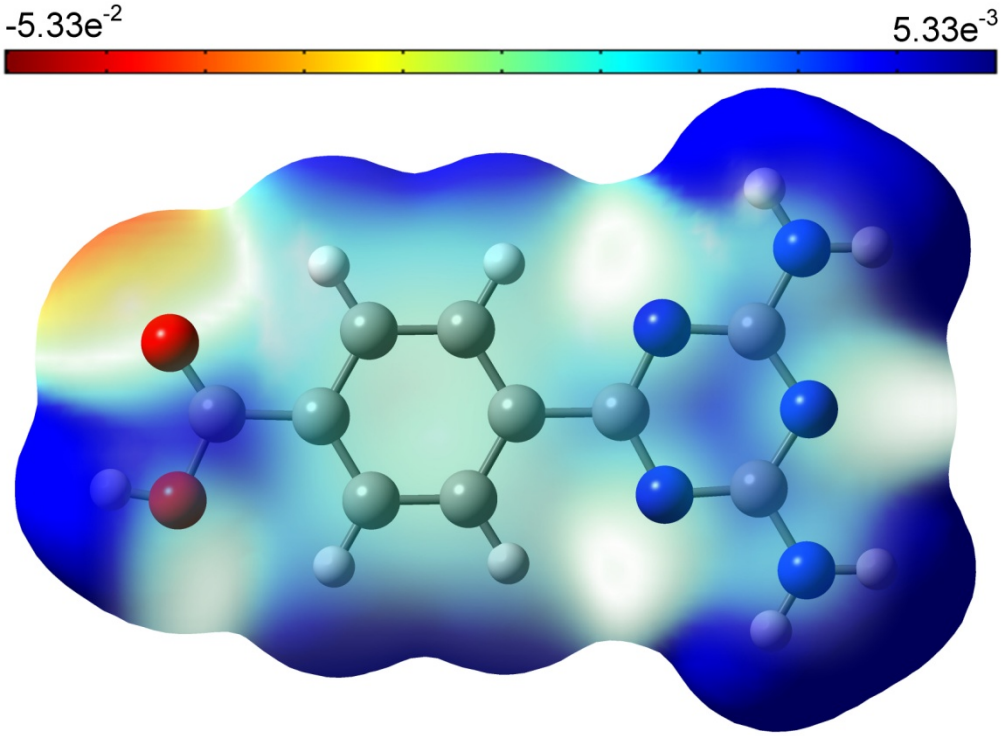

Figure S2: Electrostatic potential surface for the ligand (LH) representative of the electron density map.

Table S1. Physical Properties of C_6 adsorptive species.

Dimensions of Adsorptive molecules (Å)[S6] (each atom surrounded by a van der Waals sphere) Dimensional Closeness						Boiling and Freezing Points		Conformers
	x	***y***	**z**	**MIN-1**	**MIN-2**	**B.P.**	**F.P.**	**Type(s)**
Bz	6.628	7.337	3.277	3.277	6.628	353.3 K	278.7 K	Planar
Cy	7.168	6.580	4.982	4.982	6.580	353.9 K	279.6 K	Non-planar: Boat and Chair

MIN-1: Size of the adsorptive in the minimum dimension.

MIN-2: Second minimum dimension for molecular orientations that enable a molecule to enter the channel.

Table S2. Dual-site Langmuir-Freundlich parameters for aromatic hydrocarbons at 298 K in DAT-MOF-1.

	Site A			Site B		
	$q_{i,A,sat}$ mol kg^{-1}	$b_{i,A}$ Pa$^{-\nu_{iA}}$	$\nu_{i,A}$ dimensionless	$q_{i,B,sat}$ mol kg^{-1}	$b_{i,B}$ Pa$^{-\nu_{iA}}$	$\nu_{i,B}$ dimensionless
Bz	0.85	3.1×10^{-2}	0.7	3	3.7×10^{-16}	3.6
Cy	0.5	9.55×10^{-5}	0.8	0.5	2.01×10^{-25}	6

Experimental Section:

Materials: All the reagents and solvents were commercially available and used without further purification.

Synthesis of Ligand (LH): 4-cyano benzoic acid (5g, 33.98 mmol) and dicyanamide (4.1619 g, 49.49 mmol) were added to a stirring solution of potassium hydroxide (2.772, 49.5 mmol) in 2- methoxy ethanol (100 ml) in a round bottomed flask. Resulting mixture was refluxed at 423K for 30 h. This mixture was subsequently cooled down to room temperature. The solution was neutralized using dilute HCl until the pH of reaction mixture was ~7 to get white precipitate. Then the resulting solution was filtered off, dried under vacuum to get white powder. The compound was characterized using ^{1}H NMR, ^{13}C NMR and HRMS. ^{1}H NMR (400 MHz, DMSO-d_6): δ 8.3 (td, J = 1.6, 8.8 Hz, 2H); 8.0 (td, J = 2.0, 8.8 Hz, 2H), 6.8 (S, 4H); ^{13}C NMR (100 MHz, $CDCl_3$): δ 169.4, 167.4, 167.1, 141.0, 133.1, 129.2, 127.7; HRMS (ESI): Calc. for $C_{10}H_{10}N_5O_2$ $[M+H]^+$: 232.083; Found: 232.083.

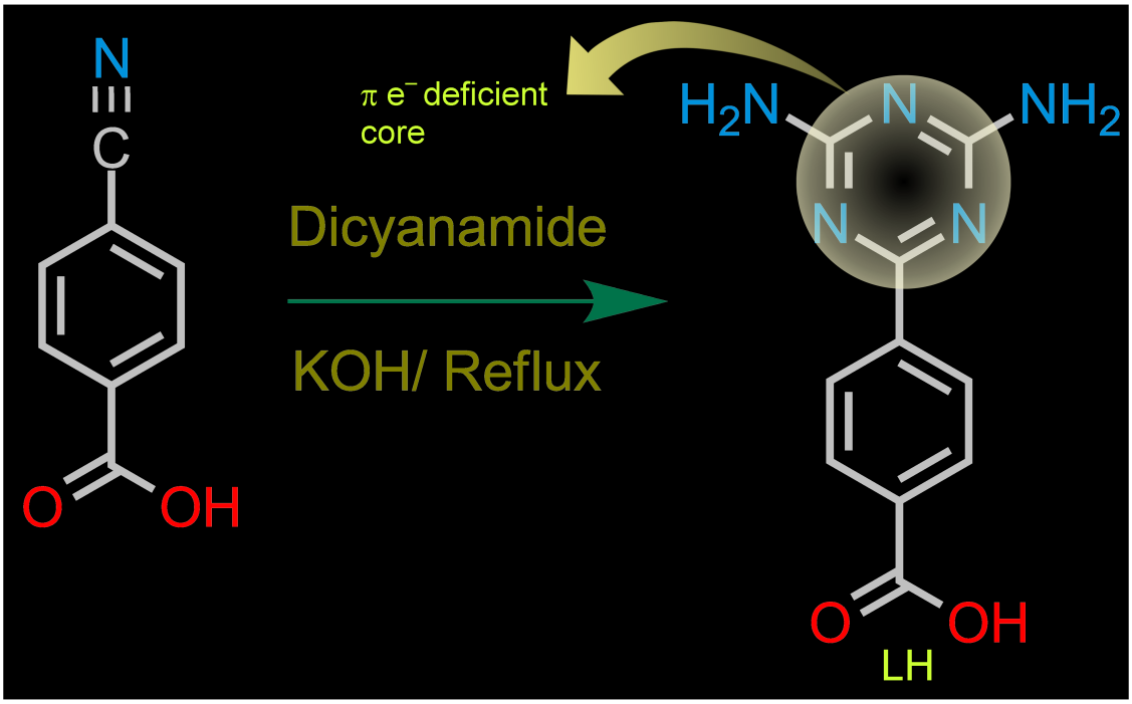

Figure S3: Ligand (LH) synthesis protocol.

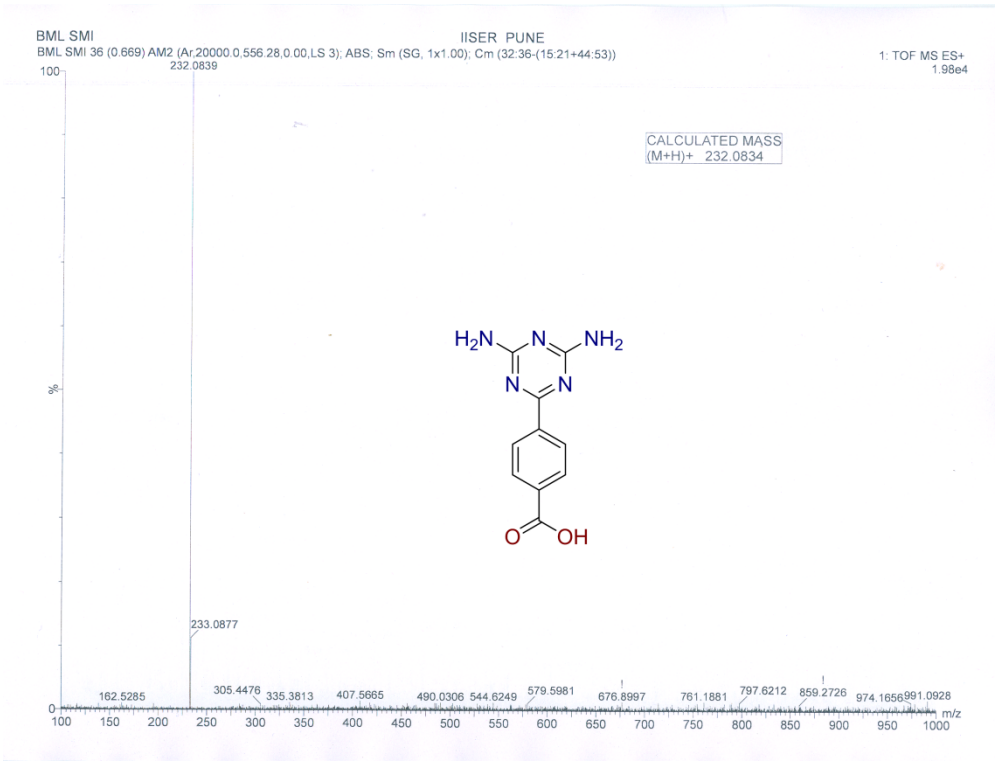

Figure S4: HRMS of ligand (LH).

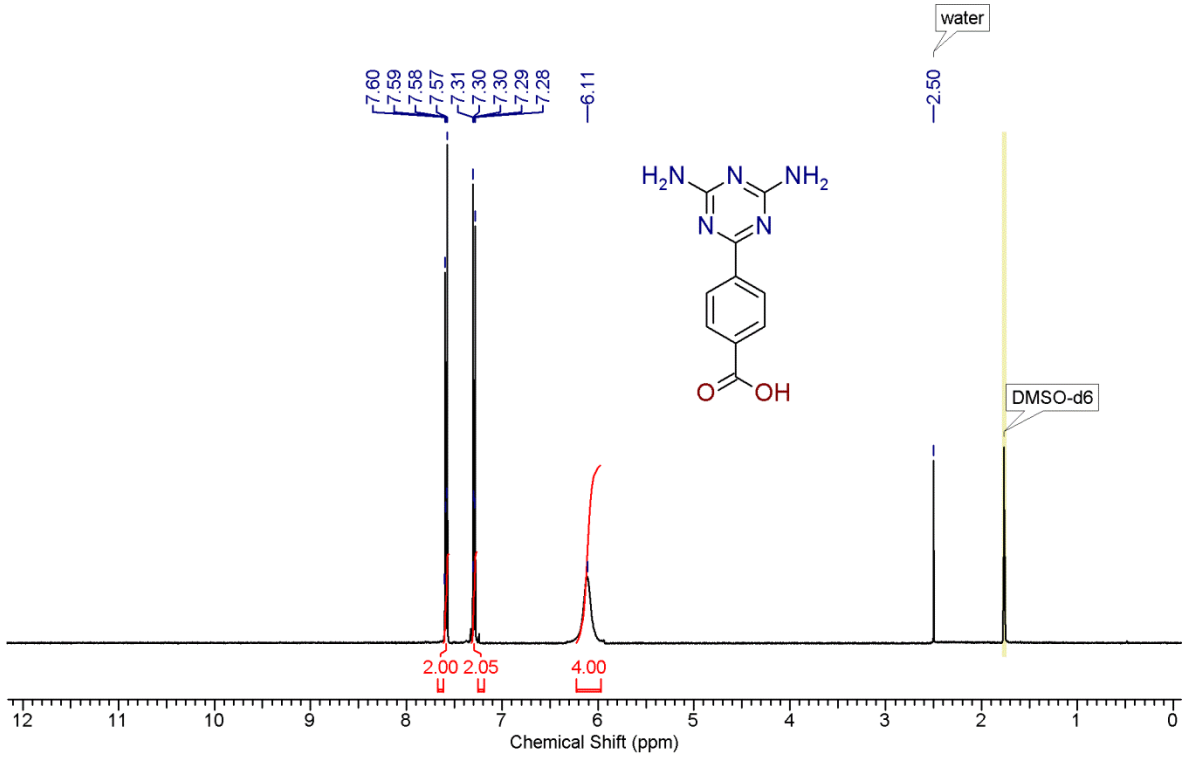

Figure S5: ^{1}H NMR of ligand (LH).

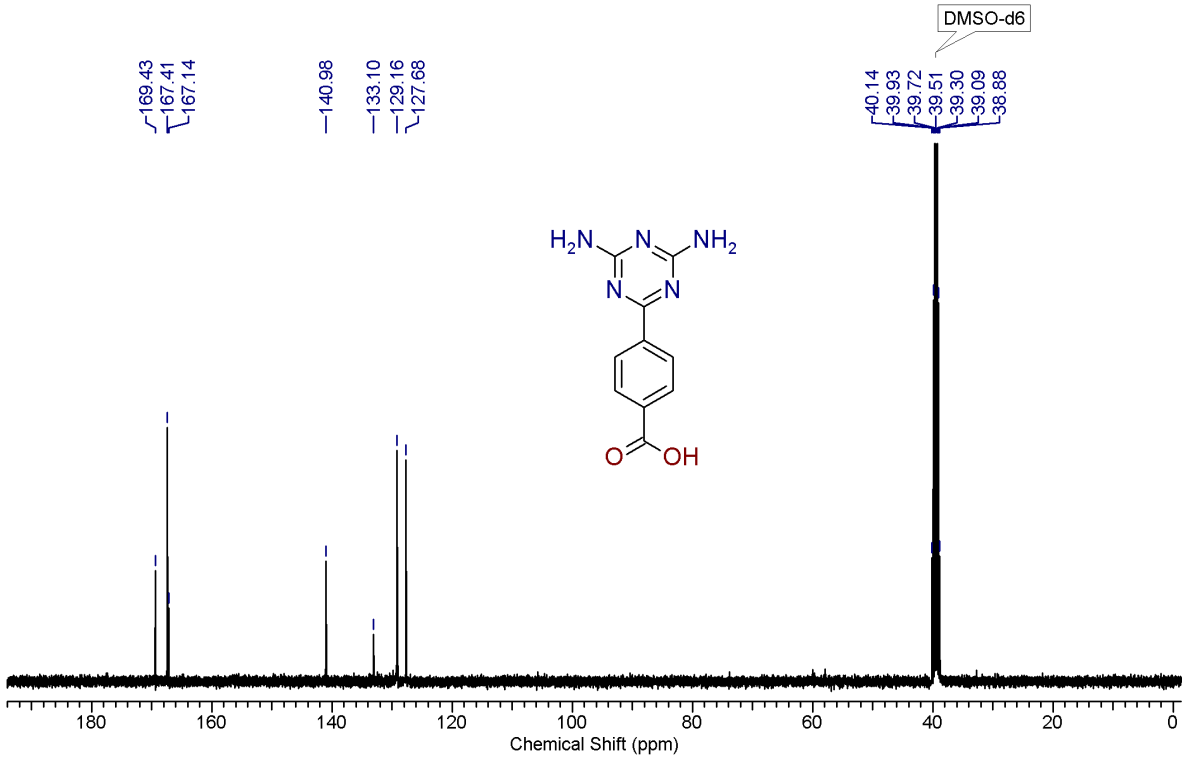

Figure S6: ^{13}C NMR of ligand (LH).

Synthesis of DAT-MOF-1a: Single crystals of DAT-MOF-1a were synthesized by reacting $Cu(NO_3)_2.3H_2O$ (0.012 g, 0.05 mmol), LH (0.0231 g, 0.1 mmol) in DMF (2 mL) and MeOH (1mL) in a 5 ml screw-capped vial. The vial was heated to 90 °C for 48h under autogenous pressure and then cooled to RT over 12 h. The green block shaped single crystals of DAT-MOF-1a were obtained with ~50% yield. Anal. found (elemental analysis) for DAT-MOF-1a (%): C, 46.92; H, 5.23; N, 22.88.

Physical measurements: Powder X-ray diffraction (PXRD) patterns were measured on Bruker D8 Advanced X-Ray diffractometer at room temperature using Cu-Kα radiation (λ= 1.5406 Å) with a scan speed of 0.5° min^{-1} and a step size of 0.01° in 2 *theta*. Thermogravimetric analysis was recorded on Perkin-Elmer STA 6000, TGA analyser under N_2 atmosphere with heating rate of 10° C/min. The IR-spectra were recorded on a *Thermoscientific*–Nicolet-6700 FT-IR spectrometer. FT-IR spectra were recorded on NICOLET 6700 FT-IR Spectrophotometer using KBr Pellets.

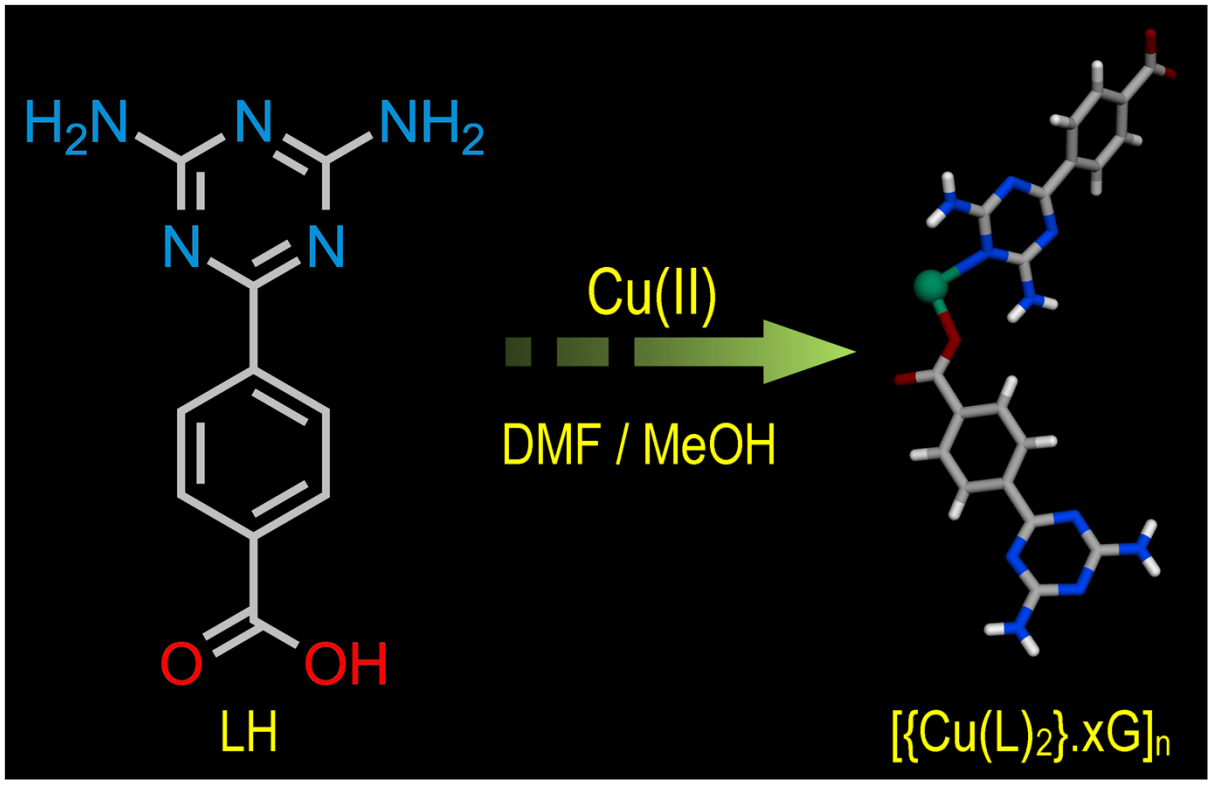

Figure S7: Synthetic scheme of DAT-MOF-1a.

X-ray Structural Studies: Single-crystal X-ray data of DAT-MOF-1a was collected at 150 K on a Bruker KAPPA APEX II CCD Duo diffractometer (operated at 1500 W power: 50 kV, 30 mA) using graphite-monochromated Mo Kα radiation (λ = 0.71073 Å). Crystal was on nylon CryoLoops (Hampton Research) with Paraton-N (Hampton Research). The data integration and reduction were processed with SAINT[S1] software. A multi-scan absorption correction was applied to the collected reflections. The structure was solved by the direct method using SHELXTL[S2] and was refined on F^2 by full-matrix least-squares technique using the SHELXL-97[S3] program package within the WINGX[S4] programme. All non-hydrogen atoms were refined anisotropically. All hydrogen atoms were located in successive difference Fourier maps and they were treated as riding atoms using SHELXL default parameters. The structures were examined using the *Adsym* subroutine of PLATON[S5] to assure that no additional symmetry could be applied to the models.

Electron density plot for Ligand (LH): Electrostatic potential surface calculation was performed with the Gaussian09 Rev D program suite using Density functional theory (DFT) with Becke's three-parameter hybrid exchange functional and the Lee-Yang-Parr correlation functional (B3LYP) and 6-31G(d,p) basis set.

Low-Pressure Gas and Solvent Sorption Measurements. Low-pressure solvent (Benzene and Cyclohexane) sorption measurements were performed using BelAqua (Bel Japan). Low pressure gas adsorption measurements were performed using BelSorpmax (Bel Japan). All the gases used were of 99.999% purity. As-synthesized crystals of compound DAT-MOF-1a were exchanged thrice each day over a period of five days with fresh batches of lower-boiling solvent acetone, before heating it under vacuum to end up with guest-free crystalline phase DAT-MOF-1.

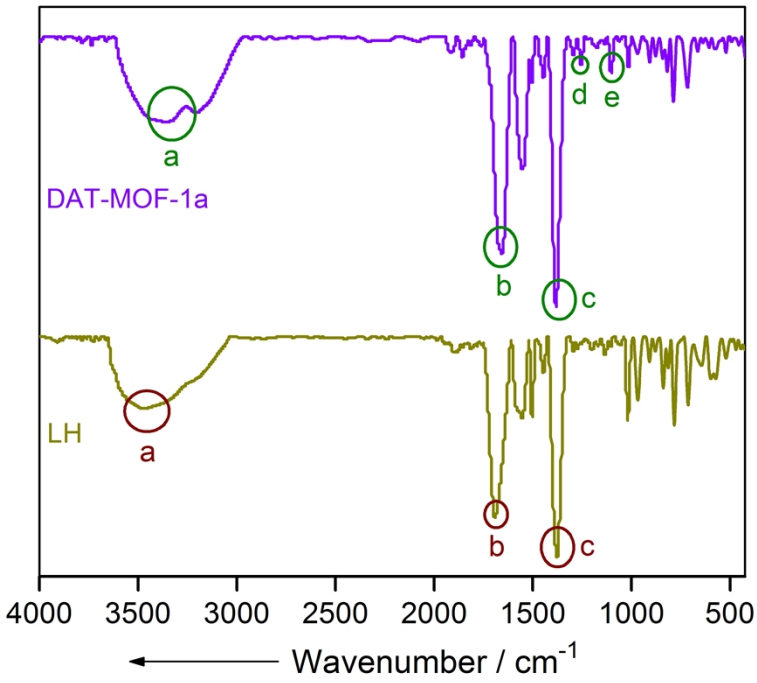

Figure S8: IR spectra of DAT-MOF-1a and the monocarboxylic acid ligand (LH), wherein the labelled peaks refer to the presence of N.N.-dimethyl formamide (DMF) molecules within DAT-MOF-1a, present in addition to the coordinated monocarboxylate diaminotriazine linker L. a: N-H stretching (also in DMF); b: C-O stretching (also in DMF); c: C-H stretching (also in DMF); d: C-N stretching (DMF); e: C-H rocking (in DMF, $-CH_3$).

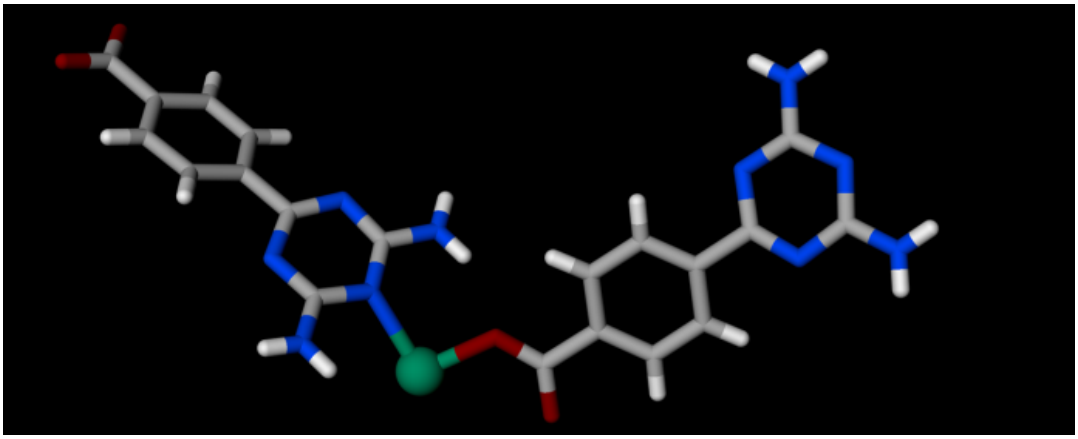

Figure S9: Asymmetric unit of DAT-MOF-1a (Color code: Carbon: grey, oxygen: red, nitrogen: blue, copper: deep green).

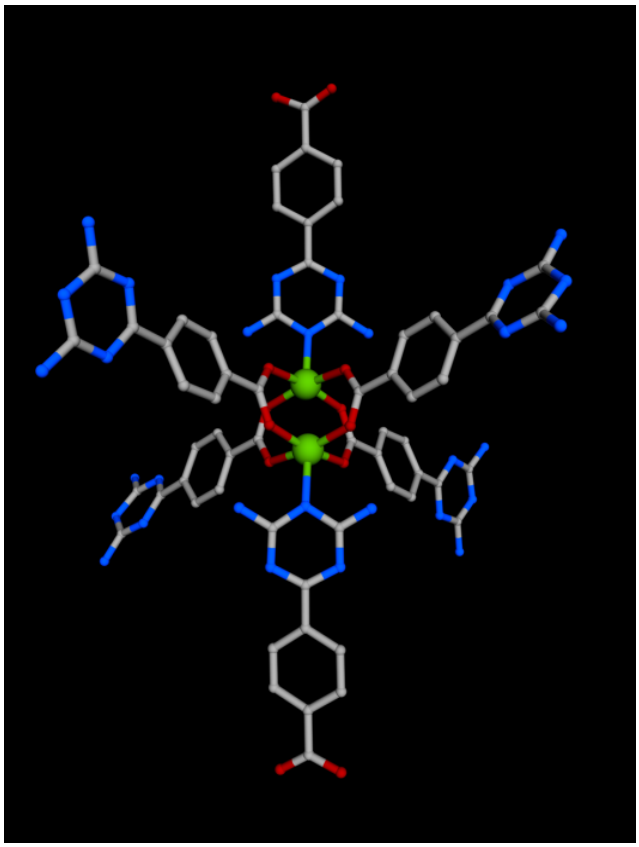

Figure S10: Coordination environment around the metal centre of DAT-MOF-1a (Color code; Carbon: grey, oxygen: red, nitrogen: blue, copper: green).

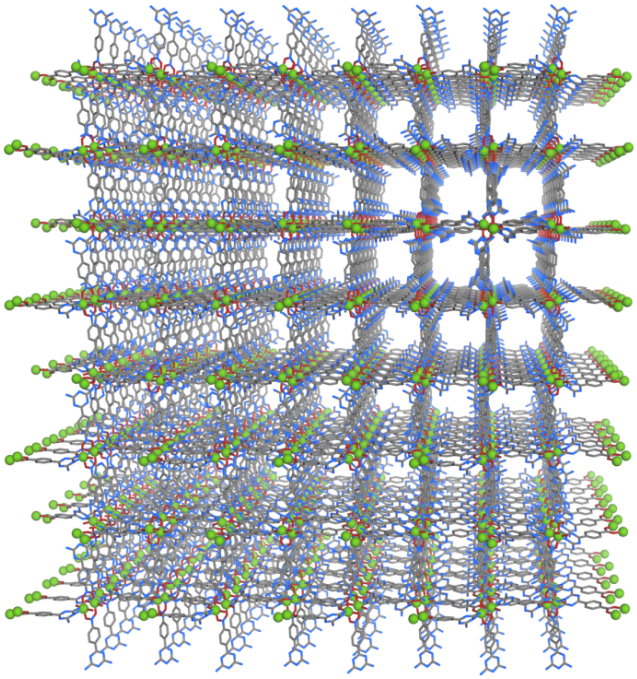

Figure S11: Perspective view of overall packing of DAT-MOF-1a along *a* axis (free guests have been omitted for clarity) (Color code; Carbon: grey, oxygen: red, nitrogen: blue, copper: green).

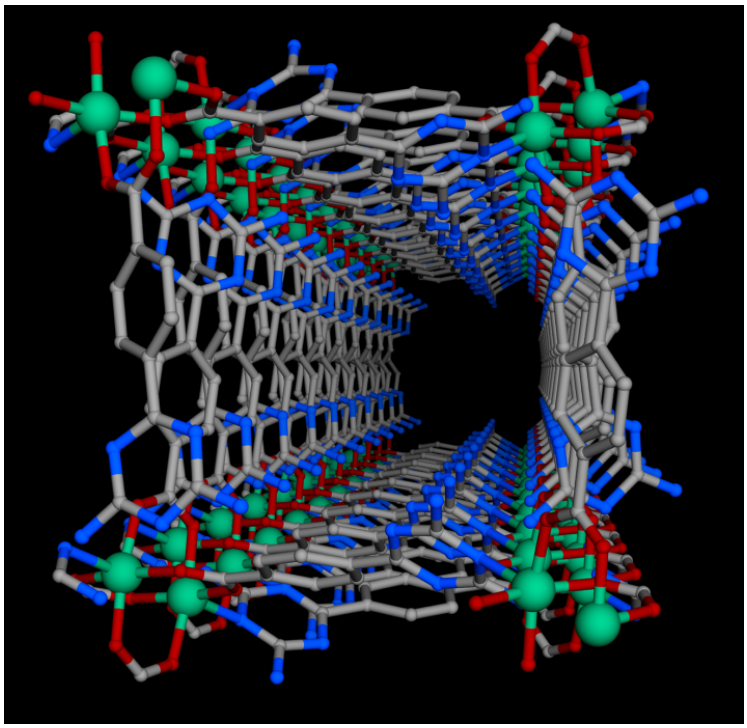

Figure S12: Perspective view of a single pore of DAT-MOF-1a along *a* axis (free guests have been omitted for clarity) (Color code; Carbon: grey, oxygen: red, nitrogen: blue, copper: green).

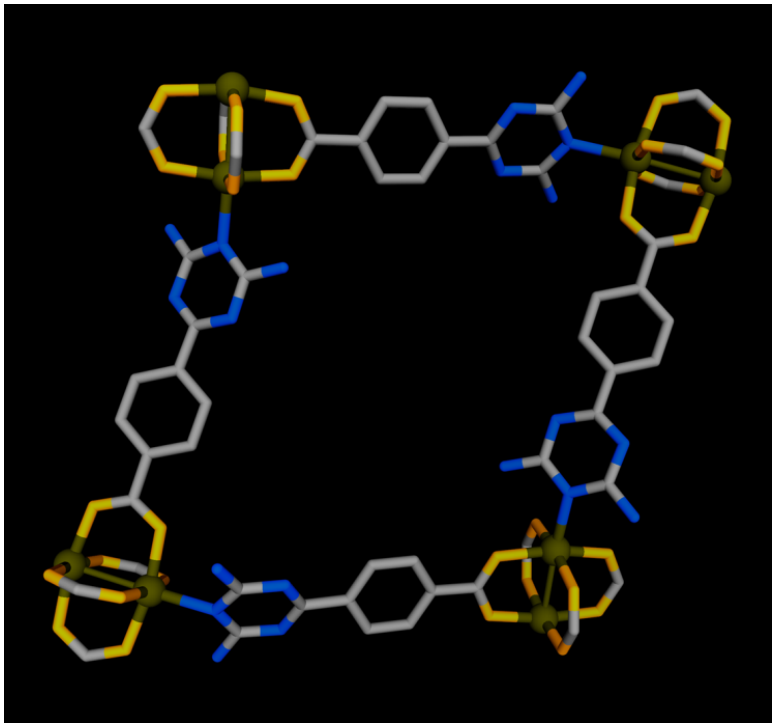

Figure S13: Single 2D net of DAT-MOF-1a *a* axis (Color code; Carbon: grey, oxygen: pale orange, nitrogen: blue, copper: dark yellow).

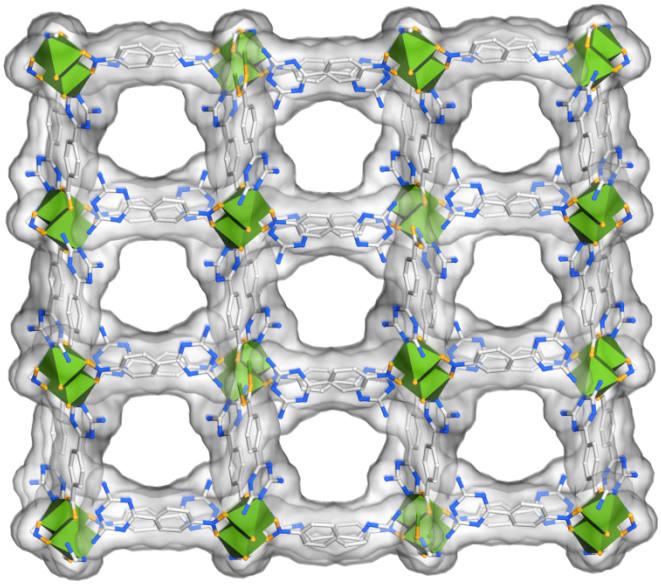

Figure S14: Pore surface of DAT-MOF-1a along *a* axis (Color code; Carbon: grey, oxygen: pale orange, nitrogen: blue, copper: green polyhedral).

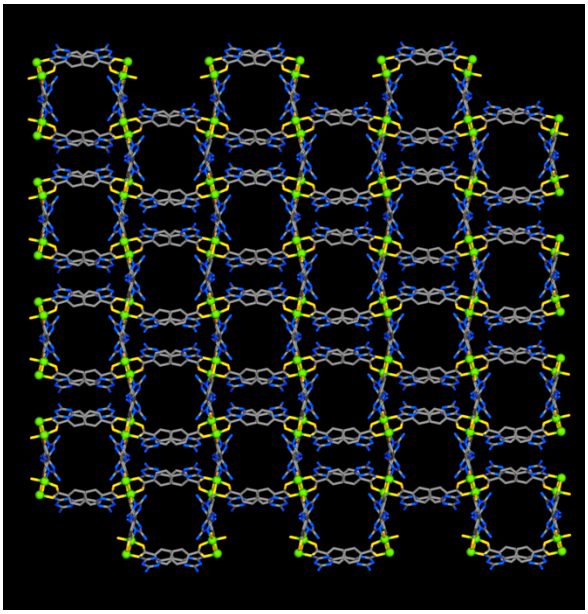

Figure S15: Overall packing along *b* axis of DAT-MOF-1a (free guests have been omitted for clarity) (Color code; Carbon: grey, oxygen: pale orange, nitrogen: blue, copper: green ball).

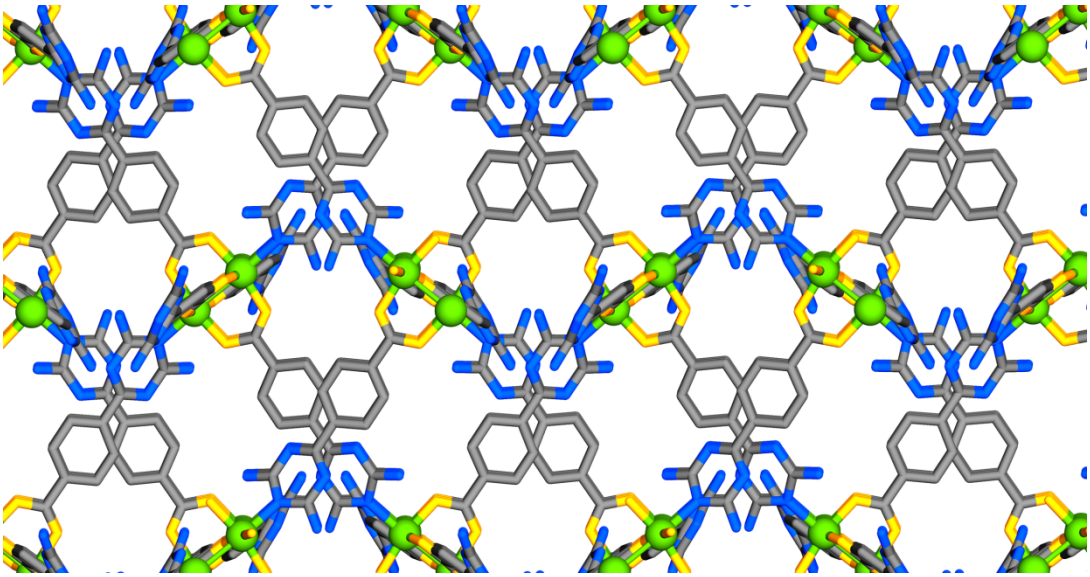

Figure S16: Overall packing along *b* axis of DAT-MOF-1a (free guests have been omitted for clarity) (Color code; Carbon: grey, oxygen: pale orange, nitrogen: blue, copper: green ball).

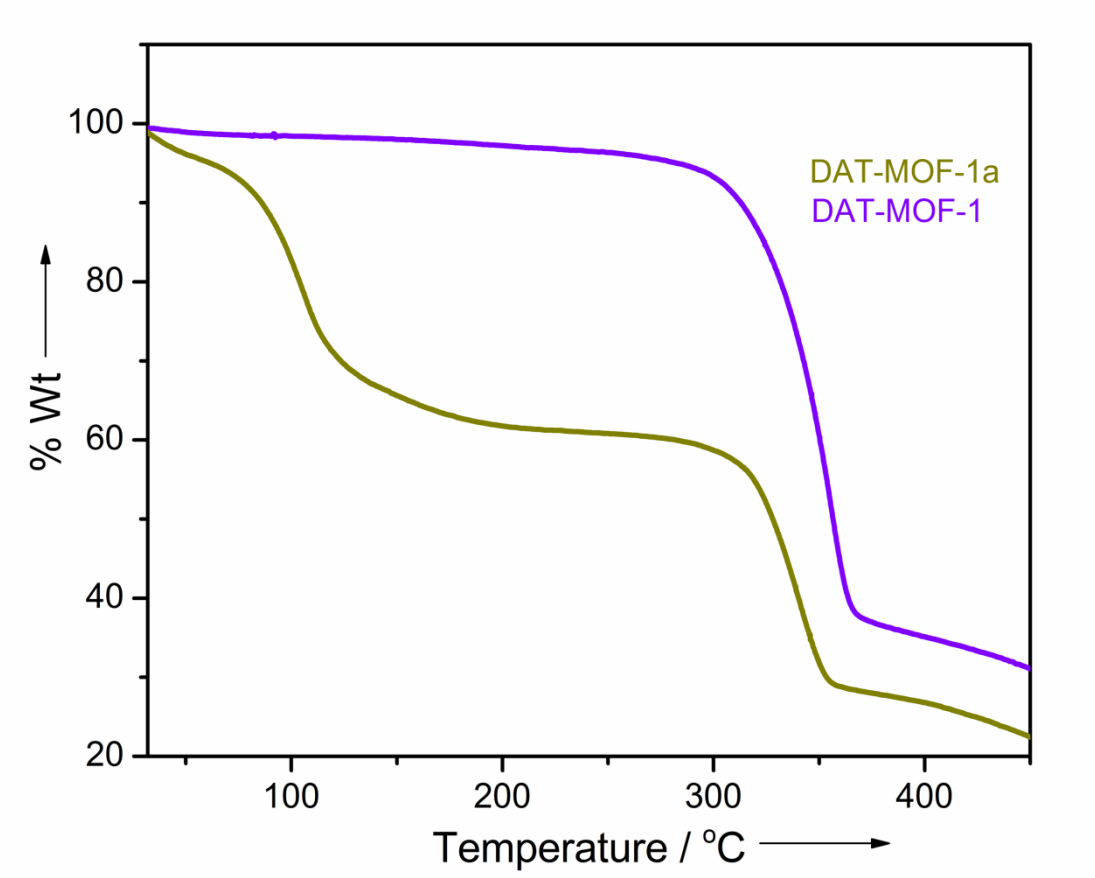

Figure S17: TGA plot of as-made and desolvated phases of DAT-MOF-1a.

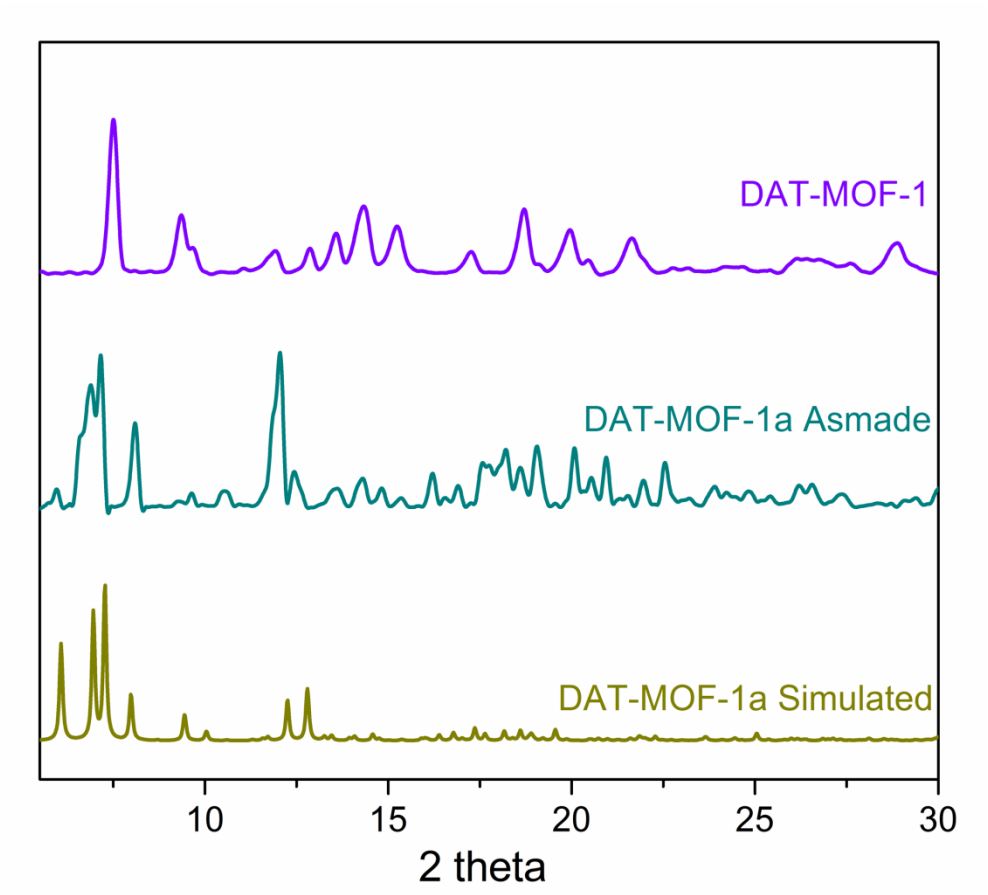

Figure S18: PXRD patterns of simulated, as-made and desolvated phases of DAT-MOF-1a.

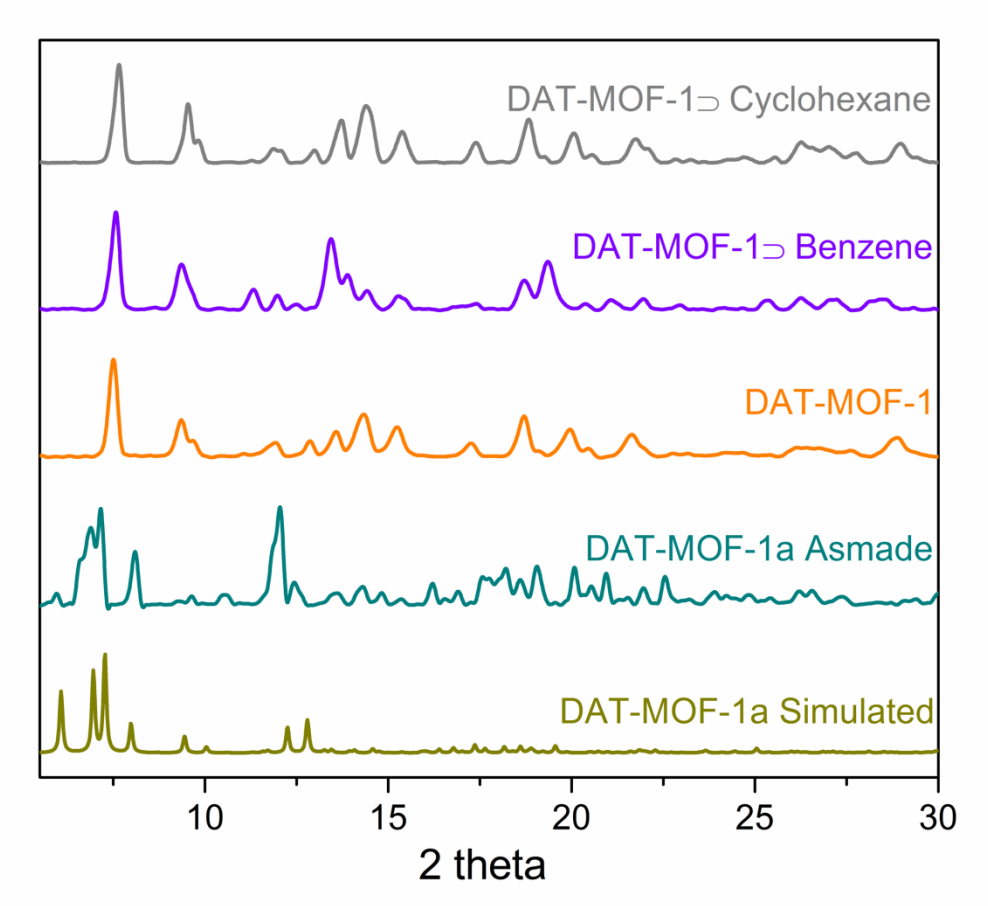

Figure S19: PXRD patterns for the Bz and Cy-vapor exposed phases of DAT-MOF-1, when compared together with the simulated and as-made patterns for DAT-MOF-1a.

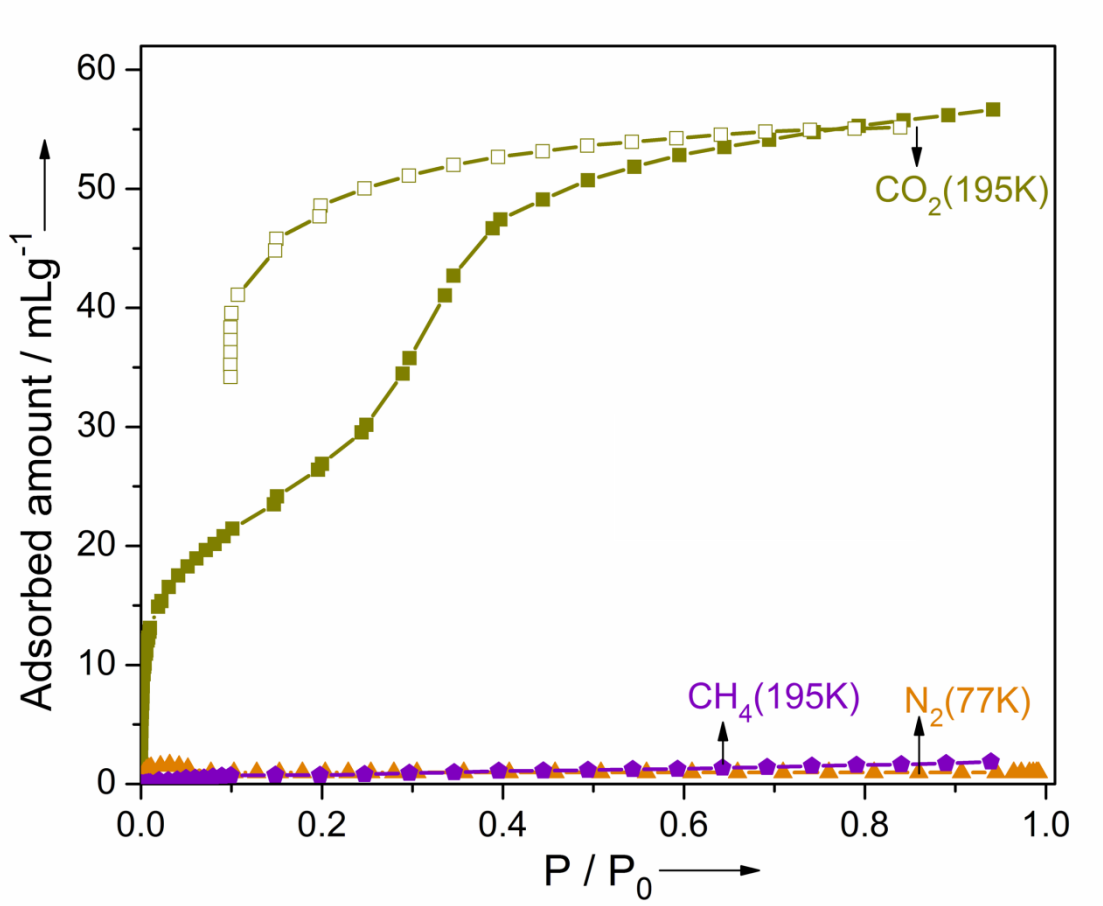

Figure S20: Low-temperature gas adsorption isotherms for DAT-MOF-1.

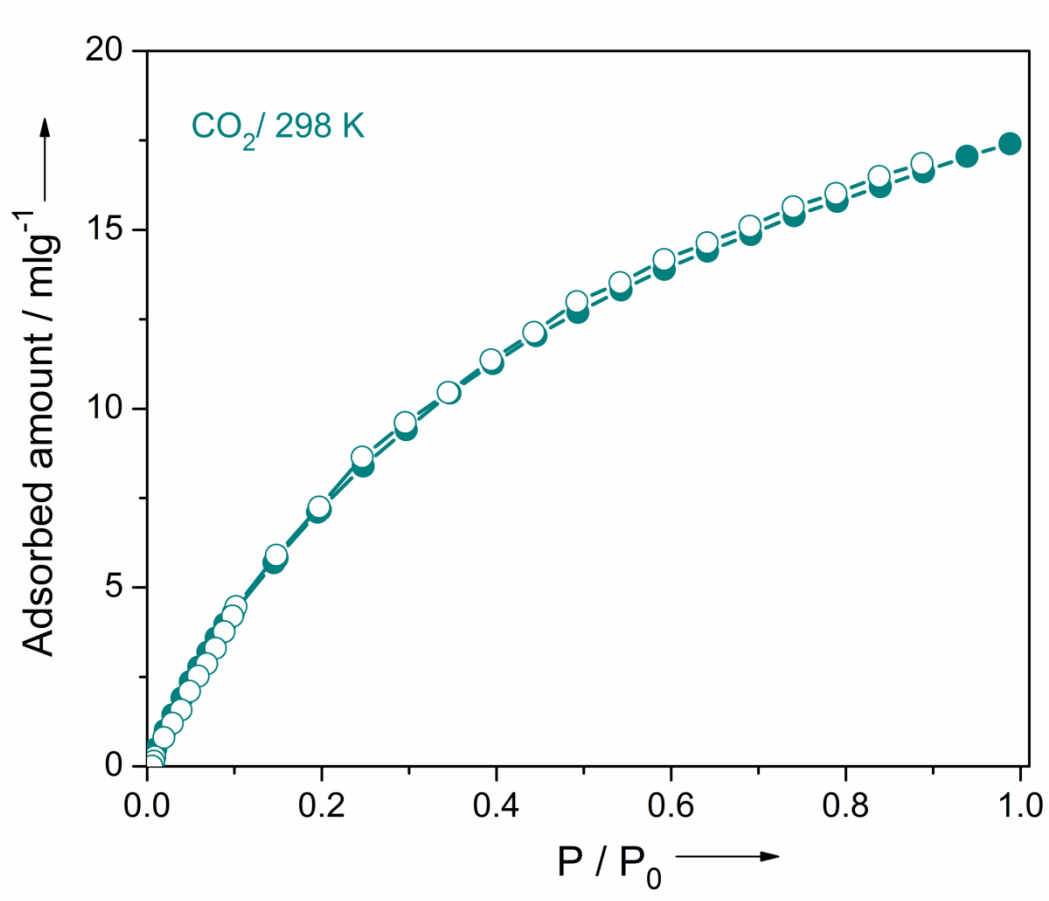

Figure S21: Room temperature CO_2 adsorption isotherms for DAT-MOF-1.

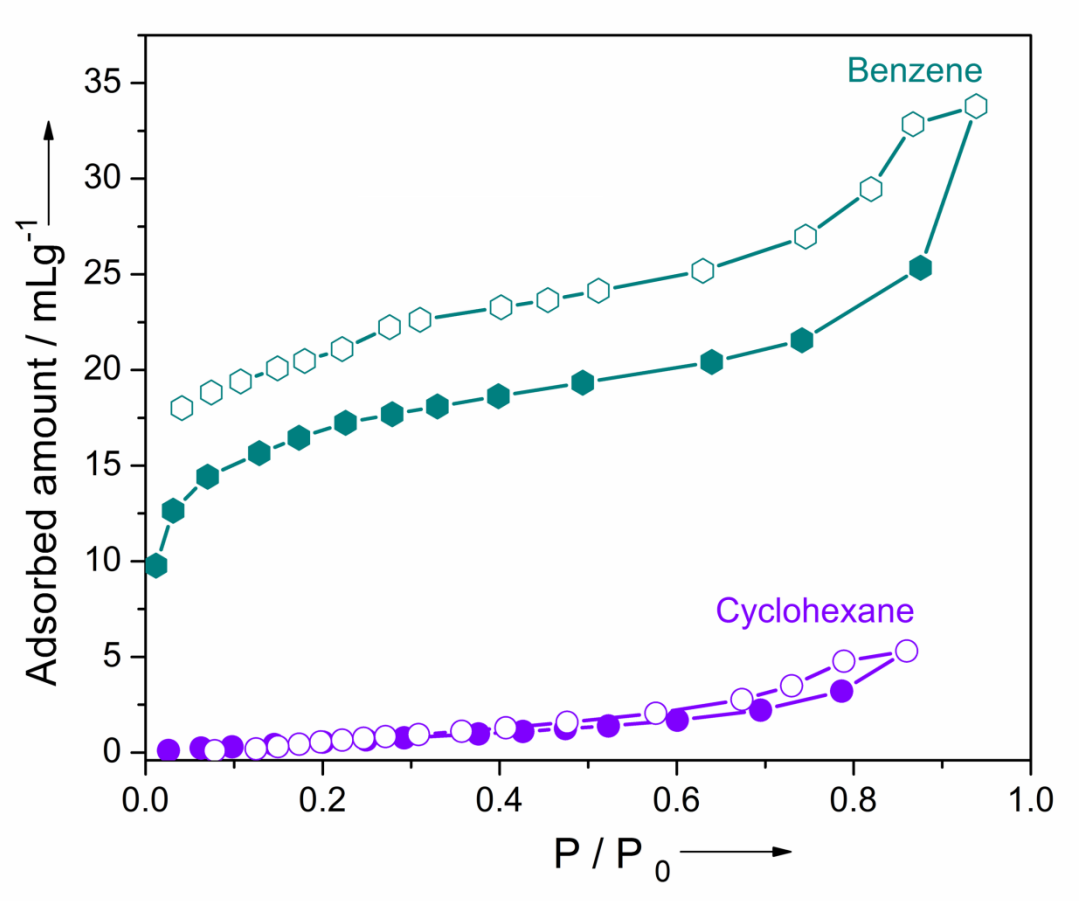

Figure S22: Benzene and Cyclohexane sorption isotherms for the desolvated phase DAT-MOF-1 recorded at 298K and 1atm.

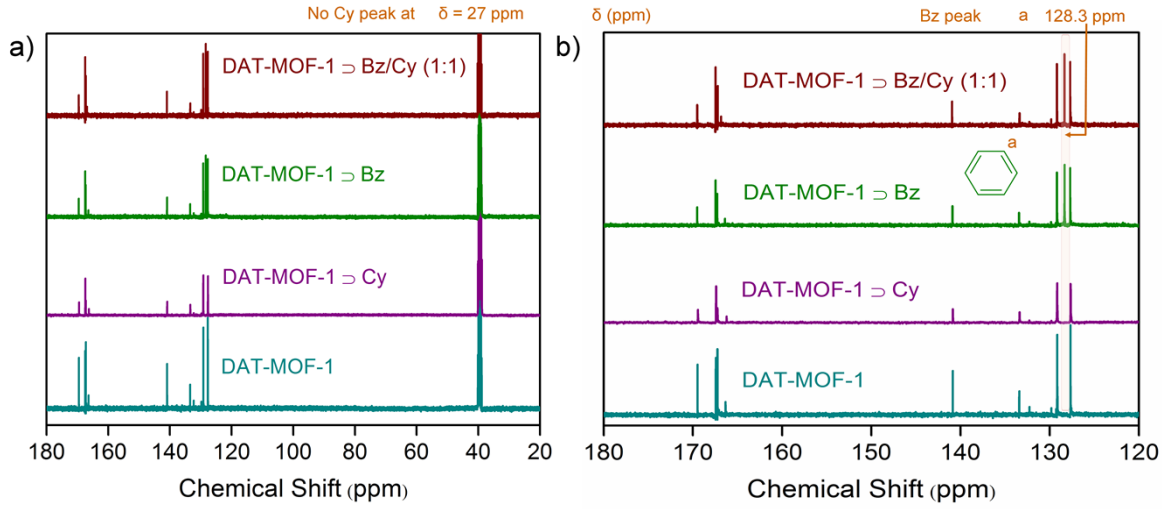

Figure S23: ^{13}C NMR spectra for Bz and Cy vapor-exposed phases of compound DAT-MOF-1, as compared to the desolvated phase itself. Vapor of each of these two solvents were exposed for 48h to the phase DAT-MOF-1 before digesting in DCl/DMSO- d_6. a) Extended ^{13}C NMR view showing no Cy peak at the characteristic cyclohexane region (δ = 27 ppm); while b) zoomed ^{13}C NMR view presenting Bz peaks for the Bz and Bz/Cy (1:1) vapor exposed phases observed at Bz characteristic region (δ = 128.3 ppm).

Table S3. Crystal data and structure refinement for DAT-MOF-1a.

Identification code	DAT-MOF-1a	
Empirical formula	$C_{20}\ H_{16}\ Cu\ N_{10}\ O_4$	
Formula weight	523.97	
Temperature	100(2) K	
Wavelength	0.71073 Å	
Crystal system	Orthorhombic	
Space group	*P b n b*	
Unit cell dimensions	a = 17.7157(6) Å	α= 90°.
	b = 22.1231(8) Å	β= 90°.
	c = 25.3814(9) Å	γ= 90°.
Volume	9947.6(6) Å^3	
Z	8	
Density (calculated)	0.700 Mg/m^3	
Absorption coefficient	0.462 mm^{-1}	
F(000)	2136	
Crystal size	0.15 x 0.11 x 0.10 mm^3	
Theta range for data collection	1.40 to 25.41°.	
Index ranges	-21<=h<=21, -23<=k<=26, -30<=l<=30	
Reflections collected	163610	
Independent reflections	9132 [R(int) = 0.0919]	
Completeness to theta = 25.41°	99.4 %	
Absorption correction	Semi-empirical from equivalents	
Max. and min. transmission	0.9552 and 0.9339	
Refinement method	Full-matrix least-squares on F^2	
Data / restraints / parameters	9132 / 0 / 316	
Goodness-of-fit on F^2	0.963	
Final R indices [I>2sigma(I)]	R_1 = 0.0656, wR2 = 0.1540	
R indices (all data)	R_1 = 0.0814, wR2 = 0.1646	
Largest diff. peak and hole	1.273 and -0.315 e.Å^{-3}	

Table S4. Atomic coordinates (x 10^4) and equivalent isotropic displacement parameters ($Å^2$x 10^3) for DAT-MOF-1a. U(eq) is defined as one third of the trace of the orthogonalized U^{ij} tensor.

	x	y	z	U(eq)
Cu(01)	9438(1)	362(1)	144(1)	34(1)
O(4)	10190(1)	994(1)	35(1)	42(1)
O(2)	8845(1)	-396(1)	189(1)	33(1)
O(1)	9855(1)	210(1)	847(1)	39(1)
O(3)	9201(1)	408(1)	-615(1)	40(1)
N(7)	8561(1)	980(1)	424(1)	25(1)
N(9)	7650(1)	481(1)	-47(1)	34(1)
N(6)	8291(1)	1992(1)	694(1)	32(1)
N(8)	7436(1)	1469(1)	127(1)	29(1)
N(2)	11406(2)	-536(1)	4180(1)	44(1)
C(18)	7681(2)	1961(1)	387(1)	28(1)
N(10)	9310(1)	1482(1)	1017(1)	43(1)
N(3)	11490(2)	-914(1)	3294(1)	48(1)
C(19)	8709(2)	1489(1)	706(1)	29(1)
C(13)	7094(2)	3603(1)	341(1)	33(1)
C(20)	7881(1)	979(1)	174(1)	25(1)
C(16)	6480(2)	2469(1)	142(1)	39(1)
N(4)	11972(2)	-1430(1)	3986(1)	53(1)
C(14)	7524(2)	3090(1)	411(1)	38(1)
C(1)	10405(2)	-132(1)	946(1)	34(1)
C(15)	7228(2)	2512(1)	309(1)	30(1)
C(7)	11223(2)	-551(1)	1662(1)	43(1)
N(1)	10886(2)	27(2)	3459(1)	59(1)
C(12)	6350(2)	3552(1)	166(1)	33(1)
C(2)	10620(2)	-205(2)	1514(1)	42(1)
C(8)	11114(2)	-411(2)	3151(1)	51(1)
C(11)	5866(2)	4104(1)	104(1)	29(1)
C(9)	11036(2)	-47(2)	3983(1)	53(1)
C(10)	11612(2)	-948(1)	3814(1)	41(1)
C(6)	11399(2)	-624(2)	2200(1)	44(1)
C(17)	6048(2)	2985(1)	57(1)	37(1)
C(3)	10173(2)	66(2)	1897(1)	71(1)
N(5)	10832(2)	371(2)	4316(1)	72(1)

C(5)	10955(2)	-351(2)	2572(1)	53(1)
C(4)	10340(2)	10(2)	2423(2)	70(1)

Table S5. Bond lengths [Å] and angles [°] for DAT-MOF-1a.

Cu(01)-O(4)	1.9522(19)
Cu(01)-O(1)	1.9585(19)
Cu(01)-O(3)	1.975(2)
Cu(01)-O(2)	1.9824(18)
Cu(01)-N(7)	2.190(2)
Cu(01)-Cu(01)#1	2.6563(7)
O(4)-C(11)#2	1.267(3)
O(2)-C(11)#3	1.238(3)
O(1)-C(1)	1.258(3)
O(3)-C(1)#1	1.252(4)
N(7)-C(19)	1.358(3)
N(7)-C(20)	1.362(3)
N(9)-C(20)	1.303(3)
N(6)-C(18)	1.332(3)
N(6)-C(19)	1.338(3)
N(8)-C(20)	1.345(3)
N(8)-C(18)	1.345(3)
N(2)-C(10)	1.351(4)
N(2)-C(9)	1.359(4)
C(18)-C(15)	1.472(3)
N(10)-C(19)	1.325(4)
N(3)-C(10)	1.340(4)
N(3)-C(8)	1.346(4)
C(13)-C(14)	1.378(4)
C(13)-C(12)	1.395(4)
C(16)-C(17)	1.391(4)
C(16)-C(15)	1.395(4)
N(4)-C(10)	1.316(4)
C(14)-C(15)	1.407(4)
C(1)-O(3)#1	1.252(4)
C(1)-C(2)	1.500(4)
C(7)-C(2)	1.367(4)
C(7)-C(6)	1.409(5)
N(1)-C(8)	1.310(5)
N(1)-C(9)	1.367(5)
C(12)-C(17)	1.392(4)

C(12)-C(11)	1.501(3)
C(2)-C(3)	1.390(5)
C(8)-C(5)	1.502(4)
C(11)-O(2)#4	1.238(3)
C(11)-O(4)#5	1.267(3)
C(9)-N(5)	1.305(5)
C(6)-C(5)	1.369(5)
C(3)-C(4)	1.372(5)
C(5)-C(4)	1.404(5)

O(4)-Cu(01)-O(1)	89.72(10)
O(4)-Cu(01)-O(3)	88.21(10)
O(1)-Cu(01)-O(3)	167.78(9)
O(4)-Cu(01)-O(2)	167.58(8)
O(1)-Cu(01)-O(2)	90.14(9)
O(3)-Cu(01)-O(2)	89.30(9)
O(4)-Cu(01)-N(7)	94.72(8)
O(1)-Cu(01)-N(7)	94.53(8)
O(3)-Cu(01)-N(7)	97.64(8)
O(2)-Cu(01)-N(7)	97.67(8)
O(4)-Cu(01)-Cu(01)#1	83.18(6)
O(1)-Cu(01)-Cu(01)#1	82.25(6)
O(3)-Cu(01)-Cu(01)#1	85.54(6)
O(2)-Cu(01)-Cu(01)#1	84.49(6)
N(7)-Cu(01)-Cu(01)#1	176.15(6)
C(11)#2-O(4)-Cu(01)	124.18(16)
C(11)#3-O(2)-Cu(01)	121.74(17)
C(1)-O(1)-Cu(01)	125.23(19)
C(1)#1-O(3)-Cu(01)	120.64(17)
C(19)-N(7)-C(20)	114.7(2)
C(19)-N(7)-Cu(01)	123.44(17)
C(20)-N(7)-Cu(01)	118.36(16)
C(18)-N(6)-C(19)	114.8(2)
C(20)-N(8)-C(18)	114.8(2)
C(10)-N(2)-C(9)	114.6(3)
N(6)-C(18)-N(8)	126.2(2)
N(6)-C(18)-C(15)	118.6(2)
N(8)-C(18)-C(15)	115.3(2)

C(10)-N(3)-C(8)	113.1(3)
N(10)-C(19)-N(6)	117.9(2)
N(10)-C(19)-N(7)	117.3(2)
N(6)-C(19)-N(7)	124.7(2)
C(14)-C(13)-C(12)	119.7(2)
N(9)-C(20)-N(8)	117.4(2)
N(9)-C(20)-N(7)	118.7(2)
N(8)-C(20)-N(7)	123.9(2)
C(17)-C(16)-C(15)	120.9(3)
C(13)-C(14)-C(15)	121.3(3)
O(3)#1-C(1)-O(1)	126.3(3)
O(3)#1-C(1)-C(2)	116.8(2)
O(1)-C(1)-C(2)	117.0(3)
C(16)-C(15)-C(14)	118.2(2)
C(16)-C(15)-C(18)	120.2(2)
C(14)-C(15)-C(18)	121.6(2)
C(2)-C(7)-C(6)	120.2(3)
C(8)-N(1)-C(9)	115.6(3)
C(17)-C(12)-C(13)	120.0(2)
C(17)-C(12)-C(11)	119.5(2)
C(13)-C(12)-C(11)	120.5(2)
C(7)-C(2)-C(3)	119.6(3)
C(7)-C(2)-C(1)	121.5(3)
C(3)-C(2)-C(1)	118.8(3)
N(1)-C(8)-N(3)	127.1(3)
N(1)-C(8)-C(5)	117.5(3)
N(3)-C(8)-C(5)	115.4(3)
O(2)#4-C(11)-O(4)#5	126.3(2)
O(2)#4-C(11)-C(12)	118.2(2)
O(4)#5-C(11)-C(12)	115.5(2)
N(5)-C(9)-N(2)	117.5(3)
N(5)-C(9)-N(1)	119.4(3)
N(2)-C(9)-N(1)	123.1(3)
N(4)-C(10)-N(3)	116.8(3)
N(4)-C(10)-N(2)	116.7(3)
N(3)-C(10)-N(2)	126.5(3)
C(5)-C(6)-C(7)	119.4(3)
C(16)-C(17)-C(12)	119.8(3)

C(4)-C(3)-C(2)	121.3(3)
C(6)-C(5)-C(4)	120.7(3)
C(6)-C(5)-C(8)	122.0(3)
C(4)-C(5)-C(8)	117.3(3)
C(3)-C(4)-C(5)	118.7(3)

Symmetry transformations used to generate equivalent atoms:

#1 -x+2,-y,-z #2 x+1/2,-y+1/2,-z #3 -x+3/2,y-1/2,z

#4 -x+3/2,y+1/2,z #5 x-1/2,-y+1/2,-z

Table S6. Anisotropic displacement parameters ($Å^2 x\ 10^3$) for DAT-MOF-1a. The anisotropic displacement factor exponent takes the form: $-2\pi^2[\ h^2 a^{*2} U^{11} + ... + 2\ h\ k\ a^*\ b^*\ U^{12}\ ]$

	U^{11}	U^{22}	U^{33}	U^{23}	U^{13}	U^{12}
Cu(01)	33(1)	23(1)	47(1)	2(1)	-5(1)	-2(1)
O(4)	27(1)	18(1)	81(2)	-6(1)	12(1)	-7(1)
O(2)	24(1)	17(1)	59(1)	-2(1)	-1(1)	-1(1)
O(1)	47(1)	36(1)	33(1)	-2(1)	-16(1)	18(1)
O(3)	39(1)	46(1)	34(1)	7(1)	-11(1)	16(1)
N(7)	25(1)	12(1)	39(1)	-3(1)	-10(1)	2(1)
N(9)	30(1)	17(1)	55(2)	-10(1)	-18(1)	11(1)
N(6)	29(1)	21(1)	46(1)	-7(1)	-12(1)	7(1)
N(8)	31(1)	15(1)	41(1)	-9(1)	-6(1)	3(1)
N(2)	45(2)	44(2)	43(2)	8(1)	-16(1)	-7(1)
C(18)	28(1)	19(1)	38(2)	-5(1)	-5(1)	1(1)
N(10)	41(1)	28(1)	60(2)	-16(1)	-25(1)	13(1)
N(3)	57(2)	44(2)	43(2)	2(1)	-19(1)	6(1)
C(19)	23(1)	25(1)	40(2)	-2(1)	-6(1)	-2(1)
C(13)	25(1)	18(1)	57(2)	2(1)	-10(1)	-3(1)
C(20)	20(1)	23(1)	32(1)	2(1)	-6(1)	5(1)
C(16)	31(2)	17(1)	68(2)	-10(1)	-7(1)	3(1)
N(4)	82(2)	39(2)	39(2)	3(1)	-21(2)	5(2)
C(14)	25(1)	20(1)	69(2)	-10(1)	-12(1)	1(1)
C(1)	37(2)	24(1)	40(2)	1(1)	-10(1)	7(1)
C(15)	31(1)	18(1)	40(2)	-4(1)	-9(1)	7(1)
C(7)	46(2)	38(2)	45(2)	-2(1)	-4(2)	7(1)
N(1)	58(2)	75(2)	44(2)	0(2)	-20(1)	28(2)
C(12)	27(1)	17(1)	56(2)	-1(1)	0(1)	5(1)
C(2)	39(2)	42(2)	44(2)	6(1)	-11(1)	9(1)
C(8)	62(2)	57(2)	35(2)	0(2)	-12(2)	19(2)
C(11)	24(1)	17(1)	45(2)	-1(1)	2(1)	2(1)
C(9)	45(2)	68(2)	47(2)	3(2)	-6(2)	13(2)
C(10)	42(2)	36(2)	46(2)	1(1)	-16(1)	-5(1)
C(6)	44(2)	45(2)	43(2)	4(1)	-9(1)	10(2)
C(17)	25(1)	24(1)	61(2)	-8(1)	-12(1)	5(1)
C(3)	68(3)	104(3)	43(2)	-16(2)	-16(2)	57(3)
N(5)	76(2)	95(3)	44(2)	6(2)	-14(2)	39(2)

C(5)	61(2)	64(2)	34(2)	5(2)	-14(2)	15(2)
C(4)	65(2)	101(3)	45(2)	-6(2)	-11(2)	45(2)

Notation

b_A dual-Langmuir-Freundlich constant for species *i* at adsorption site A, $Pa^{-\nu_i}$

b_B dual-Langmuir-Freundlich constant for species *i* at adsorption site B, $Pa^{-\nu_i}$

c_i molar concentration of species *i* in fluid mixture, mol m^{-3}

c_{i0} molar concentration of species *i* in fluid mixture at inlet to adsorber, mol m^{-3}

L length of packed bed adsorber, m

n number of species in the mixture, dimensionless

p_i partial pressure of species *i* in mixture, Pa

p_t total system pressure, Pa

q_i component molar loading of species *i*, mol kg^{-1}

$q_{i,sat}$ molar loading of species *i* at saturation, mol kg^{-1}

q_t total molar loading in mixture, mol kg^{-1}

$q_{sat,A}$ saturation loading of site A, mol kg^{-1}

$q_{sat,B}$ saturation loading of site B, mol kg^{-1}

t time, s

T absolute temperature, K

u superficial gas velocity in packed bed, m s^{-1}

v interstitial gas velocity in packed bed, m s^{-1}

Greek letters

ε voidage of packed bed, dimensionless

ν exponent in dual-Langmuir-Freundlich isotherm, dimensionless

θ_t fractional occupancy within the pores, dimensionless

ρ framework density, kg m^{-3}

τ time, dimensionless

Subscripts

i	referring to component *i*
A	referring to site A
B	referring to site B
t	referring to total mixture

References:

(S1) *SAINT Plus*, (Version 7.03); Bruker AXS Inc.: Madison, WI, **2004**.

(S2) G. M. Sheldrick, *SHELXTL*, *Reference Manual*: version 5.1: Bruker AXS; Madison, WI, **1997**.

(S3) G. M. Sheldrick, *Acta Crystallogr. Sect. A* **2008**, 112 –122.

(S4) WINGX version 1.80.05 Louis Farrugia, University of Glasgow.

(S5) A. L. Spek, (2005) PLATON, *A Multipurpose Crystallographic Tool*, Utrecht University, Utrecht, The Netherlands.

(S6) C. E. Webster, R. S. Drago, M. C. Zerner, *J. Am. Chem. Soc.***1998**, *120*, 5509-5516.

N.B. ‡ B.M. and S.M. have contributed equally.